A reconstructed Siberian High index since A.D. 1599 from Eurasian and North American tree rings

Rosanne D'Arrigo,[1] Gordon Jacoby,[1] Rob Wilson,[2] and Fotis Panagiotopoulos[3]

Received 20 December 2004; revised 17 January 2005; accepted 2 February 2005; published 2 March 2005.

[1] The long-term variability of the Siberian High, the dominant Northern Hemisphere anticyclone during winter, is largely unknown. To investigate how this feature varied prior to the instrumental record, we present a reconstruction of a Dec–Feb Siberian High (SH) index based on Eurasian and North American tree rings. Spanning 1599–1980, it provides information on SH variability over the past four centuries. A decline in the instrumental SH index since the late 1970s, related to Eurasian warming, is the most striking feature over the past four hundred years. It is associated with a highly significant ($p < 0.0001$) step change in 1989. Significant ~3–4 yr spectral peaks in the reconstruction fall within the range of variability of the East Asian winter monsoon (which has also declined recently) and lend further support to proposed relationships between these large-scale features of the climate system. **Citation:** D'Arrigo, R., G. Jacoby, R. Wilson, and F. Panagiotopoulos (2005), A reconstructed Siberian High index since A.D. 1599 from Eurasian and North American tree rings, *Geophys. Res. Lett.*, *32*, L05705, doi:10.1029/2004GL022271.

1. Introduction

[2] The SH is a semi-permanent anticyclone centered over Eurasia from 40–65°N, 80–120°E (Figure 1) (see *Sahsamanoglou et al.* [1991] (hereinafter referred to as S1991) and *Panagiotopoulos et al.* [2005] (hereinafter referred to as P2005)). It is associated with some of the coldest, densest air masses in the Northern Hemisphere and is of greater intensity than the persistent pressure systems of the North Atlantic (Icelandic Low) and North Pacific (Aleutian Low) regions (S1991). Strongest in winter, the SH is maintained by radiative cooling over snow-covered Asia, associated with large-scale descending motion [*Ding and Krishnamurti*, 1987]. It is a shallow cold-core system confined to the lower troposphere below 500 mb [P2005].

[3] Relationships have been identified between the SH and Eurasian climate. Greater autumn Eurasian snow cover correlates with more intense anticyclonic conditions [*Cohen et al.*, 2001]. A correlation of $r = -0.58$ (0.01, 1922–1999) was found between the SH and Asian temperatures (30–70°N, 30–140°E), with the greatest correlations over Mongolia [*Gong and Ho*, 2002]. Correlation with precipitation for this region was $r = -0.44$ (0.01 level) for 1922–98. Precipitation correlations are coherent over large regions of Eurasia, and highest near the Urals.

[4] Despite its spatial extent, the SH has attracted less attention than other circulation features such as the North Atlantic Oscillation or NAO [S1991; *Cohen et al.*, 2001; P2005]. The SH's interactions with features of global climate, including the NAO, Arctic Oscillation (AO) [*Wu and Wang*, 2002], East Asian winter monsoon (EAWM), Aleutian Low, and El Niño-Southern Oscillation (ENSO) are still not well understood [e.g., P2005]. Of the major teleconnection patterns of the Northern Hemisphere, the SH is best correlated with the AO ($r = -0.48$, Dec–Feb 1958–98 [*Gong and Ho*, 2002]).

[5] An association between the SH and the EAWM is one example of the SH's large-scale reach. Aspects of the EAWM, including the subtropical jet over China and the North Pacific, are significantly stronger when the SH is more intense [*Zhang et al.*, 1997; P2005]. "Cold surges", which modulate the monsoon, result from southeastward movement of the SH, which causes abrupt, dramatic drops in temperature over China and south Asia [*Yihui*, 1990; *Zhang et al.*, 1997; *Gong and Ho*, 2002]. These surges can enhance convection and precipitation in the tropics [*Yihui*, 1990]. Another tropical connection is that the SH is weaker, with less frequent cold surges, during ENSO warm events. The SH's interannual variation is in good agreement with ENSO indices [*Zhang et al.*, 1997].

[6] High-resolution proxies can greatly expand our understanding of SH variability. A 1400-yr reconstruction of the spring SH based on Greenland ice core data [*Meeker and Mayewski*, 2002], one of the only such records available, shows a shift from a weaker to stronger SH in the 15th century, interpreted as the transition from the "Medieval Warm Period" to the "Little Ice Age". To add to this information, we compiled a tree ring data set with coverage over much of the region impacted by the SH, including Russia, Mongolia and China, Europe and the Mediterranean, East Asia and western North America. We then used these records to develop an annual reconstruction of a winter SH index. Below, we describe this record and its relation to the prevailing large-scale circulation.

2. Data and Analysis

2.1. Meteorological Data

[7] We used a SH index derived from global mean sea-level pressure (GMSLP) data from the GMSLP (version 2.1f) compilation, a blend of existing gridded and observed data (UK Met Office Hadley Centre, 5° × 5° [*Basnett and Parker*, 1997]). GMSLP is one of the longest such data sets presently available (1871 to 1994). The index was created by averaging the GMSLP data over the 40–65°N, 80–120°E region considered to best represent the SH [P2005] (Figure 1).

[1]Lamont-Doherty Earth Observatory, Palisades, New York, USA.
[2]School of Geosciences, Grant Institute, University of Edinburgh, Edinburgh, UK.
[3]Department of Geography, University of Reading, Reading, UK.

0094-8276/05/2004GL022271$05.00

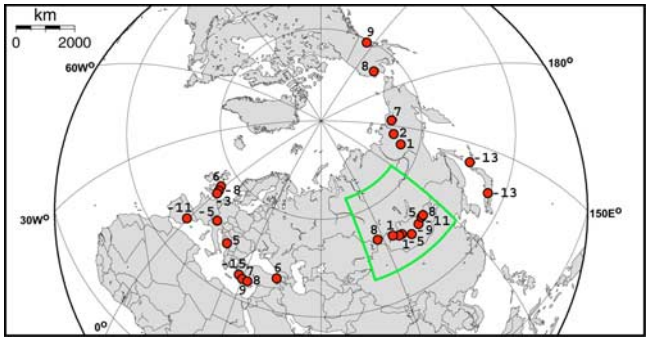

Figure 1. Map showing area (rectangle) for which global mean sea-level pressure (GMSLP) data were averaged to create SH index. Red dots show site locations (some dots represent more than 1 site) with regression weights for 1872–1980 model of most recent (1776–1980) nest.

[8] Figure 2a shows the SH GMSLP series for the Dec–Feb season of greatest intensity. A similar index generated from the *Trenberth and Paolino* [1980] gridded SLP data set (5° × 5°) spans 1899–2004 (Figure 2a). It has been used to extend the GMSLP series from 1995–2004 (correlation between the two = 0.89; 1900–1994). The indices show a slight increase from the early-middle 20th century and a steep downward trend since ~1978 [P2005]. The low levels reached during this decline are unprecedented over the instrumental record, and are not an artifact of the method used to compute SLP [P2005]. This decline has been related to recent warming over Siberia (correlation with temperature over the SH domain is r = −0.66, 0.01) [P2005]. Consistent with this theory, models project a decline in the intensity of the SH in future decades [P2005].

2.2. Tree Ring Data and Analysis

[9] 208 tree ring chronologies from SH-impacted regions were compiled and screened against the GMSLP SH index. These chronologies, from the Tree-Ring Lab at Lamont-Doherty Earth Observ., Intl. Tree-Ring Data Bank and other sources, are sensitive to temperature and/or precipitation, which may both be impacted by the SH. Highest correlations were found for the Dec–Feb season prior to growth. Tree ring data from many sites can integrate conditions during non-growing season months [e.g., *Cook et al.*, 2002]. The chronologies were autoregressively modeled to examine persistence properties [*Cook and Kairiukstis*, 1990]. The SH meteorological data do not have persistence for the years (1871–1994) and season (Dec–Feb) analyzed; thus persistence was removed from the tree ring data. To reconstruct the SH, chronologies (at lags t and t + 1) significantly correlated (0.10 level) with the instrumental record were entered as candidate predictors in principal component regression [*Cook and Kairiukstis*, 1990]. PCs having eigenvalues >1.0 were retained, and the Akaike information criterion [*Akaike*, 1974] was used to select the number of PCs entered into the regression. A nested procedure, which accounts for an overall decreasing number of chronologies back in time, was employed to develop the longest possible reconstruction. Iterative nests begin in 1599 (26 records), 1655 (28), 1690 (30), 1726 (35) and 1776 (32). For each nested model, split period calibration/verification analyses were performed over 1872–1924 and 1925–1980. The full 1872–1980 period was used to develop the final reconstruction, with the mean and variance of each nest scaled to that of the most recent nest (1776–1980) and the relevant sections for each nest spliced together. Figure 1 shows the standardized regression coefficients (beta weights [e.g., *Cook et al.*, 2002]) for the chronologies included in the most recent nested reconstruction, representing regions impacted by the SH [e.g., *Cohen et al.*, 2001; *Gong and Ho*, 2002; P2005]. One caveat is that the reconstruction provides information not only about the SH but about teleconnections outside of its immediate source region, and these teleconnections may vary over time.

3. Reconstructed SH Index

[10] The SH reconstruction (1599–1980) is shown in Figures 2b and 2c. It was extended to 2004 using instrumental data (GMSLP for 1981–1994 and *Trenberth and Paolino* [1980] for 1995–2004) after reducing the variance to that of the reconstruction and accounting for persistence [AR-2] in the post-1994 record. Calibration and verification

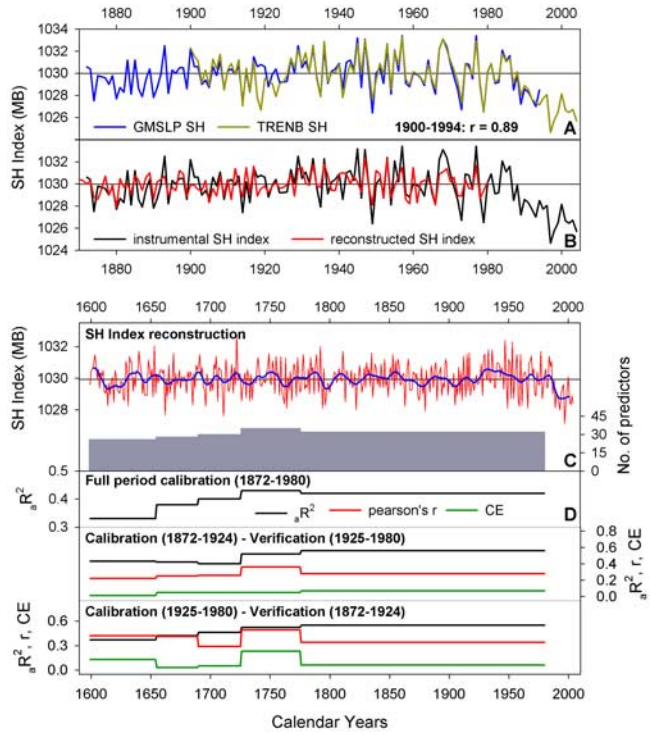

Figure 2. (a) GMSLP (1872–1994) and *Trenberth and Paolino* [1980] (1900–2004) SH indices. (b) GMSLP index and estimates for recent (1776) nest. Horizontal line (s) in Figure 2b: mean of 1900–1994 (1872–1980). (c) Reconstruction from 1599–1980 (red line), with instrumental record (adjusted to reconstruction, and for autoregression in Trenberth data post-1994) from 1981–2004. Horizontal line = mean; blue line smoothed with 15-yr spline. Shading = no. of predictors. (d) Calibration-verification results for reconstruction: ar^2, Coefficient of Efficiency (positive values are significant). Sign Test results: p = 0.05 (0.01) for most recent early (late) calibration nest; as low as p = 0.39 for earlier nests [*Cook and Kairiukstis*, 1990].

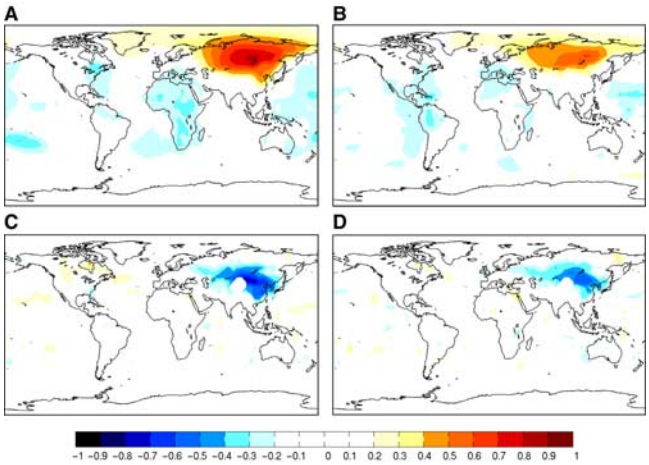

Figure 3. Correlation fields of SH index. (a) Actual and (b) estimated SH index vs. GMSLP data set; (c) actual and (d) estimated index vs. HADCRUT2 [*Jones and Moberg*, 2003] temperature data over 1872–1980 calibration period. KNMI Climate Explorer.

results [*Cook and Kairiukstis*, 1990] are shown in Figure 2d. We used the Coefficient of Efficiency, a more stringent verification statistic than the commonly used Reduction of Error [*Cook and Kairiukstis*, 1990]. The calibration ar^2 (adjusted for degrees of freedom) is 42% for the most recent (1776) nest. These tests support the reconstruction's validity in estimating the SH index over the past four centuries. However, despite the model's considerable statistical skill we consider this reconstruction to be somewhat preliminary, partly due to the need for additional coverage of tree ring data (particularly for Russia and China).

[11] The reconstruction shows considerable variability, primarily on interannual time scales. As noted, low-frequency information is limited due to prewhitening of the tree ring data; there is no persistence in the instrumental SH through to 1994. Higher intensity intervals are observed in the middle 17th and 18th centuries, and mid-20th century. Weaker conditions are reconstructed for the early 17th century and recent decades. Intervention analysis [*Box and Tiao*, 1975] was applied to identify significant step shifts in the series. This analysis was made by comparing the mean values of 10-year periods on either side of each year throughout the record. Results indicate that the recent rate of decline, associated with a highly significant ($p < 0.0001$) step change at 1989, is unprecedented over the length of the reconstruction.

[12] Spatial correlation fields were developed to compare the instrumental and reconstructed SH to the GMSLP data set (Figures 3a and 3b); and the HadCRUT2 (combined land and marine sea surface temperature or SST anomalies from the Hadley Centre of the UK Meteorological Office data set [*Jones and Moberg*, 2003]) (Figures 3c and 3d) for 1872–1980. There is good agreement, with both series showing areas of strong positive correlation with SLP and negative correlation with temperature over northern Eurasia into northeastern China. Weaker, negative SLP correlations are observed over the Mediterranean and vicinity. Weak but consistently negative correlations with SLP downstream in the subtropical Pacific may reflect the observed association between a more intense SH, a stronger EAWM and more frequent cold surges [*Wu and Wang*, 2002; *Jhun and Lee*, 2004; P2005].

[13] Multi-taper method (MTM) spectral analysis [*Mann and Lees*, 1996] was performed on the instrumental index (1872–1994), the reconstruction for the overlapping 1872–1980 interval, and the full reconstruction for 1599–2004 (Figures 4a–4c). For the recent period there are significant ~3–4 year peaks in both the actual (95%) and reconstructed (99%) series. 3–4 year peaks are also significant (95–99% level) in the full reconstruction (1599–2004; weaker in the first few centuries; not shown), with several lower frequency peaks as well. The spectral analyses show power at ~2–3 years, strongest in the full reconstruction.

4. Discussion and Conclusions

[14] We have described a reconstruction of the winter SH which provides information on past variability spanning nearly four hundred years. Based on this record, we conclude that the recent decline in the SH is the largest such shift over this interval. Interestingly, this weakening coincides with other climate changes: e.g., Eurasian warming, a North Pacific regime shift [*Trenberth*, 1990], a positive trend in the NAO/AO [*Hurrell*, 1995], and decreased coupling of the Indian monsoon and ENSO [*Kumar et al.*, 1999]. Eurasian warming associated with the SH decline may have enhanced the Eurasian land mass-Indian Ocean temperature gradient, allowing the monsoon to be maintained despite stronger recent ENSO events [*Kumar et al.*, 1999].

[15] The 3–4 year spectral peaks appear to have been a consistent feature of the SH over the past few centuries.

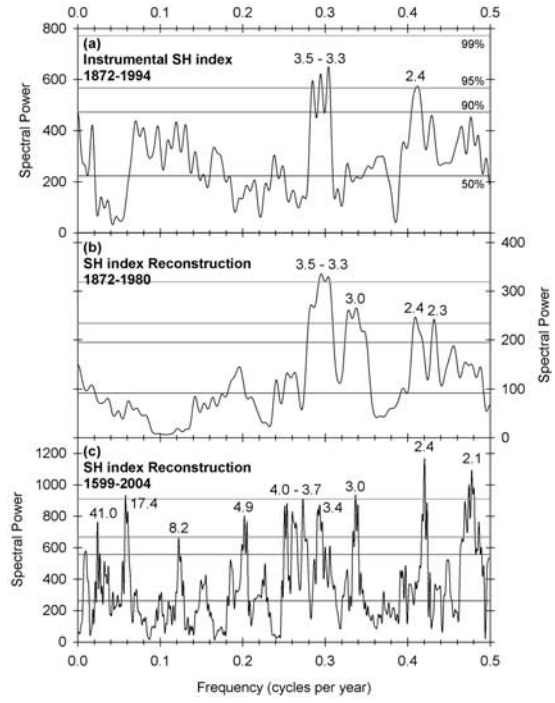

Figure 4. MTM spectral analysis of (a) GMSLP SH index from 1872–1994, (b) SH reconstruction over 1872–1980 and (c) 1599–2004.

These peaks fall within the range of variability of both ENSO [*Allan et al.*, 1996] and the EAWM [*Jhun and Lee*, 2004]. Winter precipitation over the core of the SH region is correlated with ENSO and the Indian monsoon [*Kripalani and Kulkarni*, 1999; *Morinaga et al.*, 2003]. The instrumental SH correlates with an EAWM index at r = 0.8 (1958–2000 [*Wu and Wang*, 2002]). Thus the SH reconstruction also provides important information about the EAWM, which has also declined recently [*Nakamura et al.*, 2002]. However, these relationships are complex and variable over time [e.g., *Kripalani and Kulkarni*, 1999]. Additional investigations are needed to understand these interactions and how recent shifts in these phenomena may be related to anthropogenic change.

[16] **Acknowledgments.** This research funded by NSF OCE 04-02474. We thank contributors to the International Tree-Ring Data Bank. This is LDEO contribution 6729.

References

Akaike, H. (1974), A new look at the statistical model identification, *IEEE Trans. Autom. Control*, *19*, 716–723.

Allan, R., J. Lindesay, and D. Parker (1996), *El Niño-Southern Oscillation and Climatic Variability*, 405 pp., Commonwealth Sci. and Ind. Res. Organ., Melbourne, Vic., Australia.

Basnett, T., and D. Parker (1997), Development of global mean sea level pressure data set GMSLP2, *Clim. Res. Tech. Note CRTN 79*, Hadley Centre, Exeter, U. K.

Box, G., and G. Tiao (1975), Intervention analysis with applications to economic and environmental problems, *J. Am. Stat. Assoc.*, *70*, 70–79.

Cohen, J., K. Saito, and D. Entekhabi (2001), The role of the Siberian High in Northern Hemisphere climate variability, *Geophys. Res. Lett.*, *28*, 299–302.

Cook, E., and L. Kairiukstis (1990), *Methods of Dendrochronology*, Springer, New York.

Cook, E., R. D'Arrigo, and M. Mann (2002), A well-verified, multi-proxy reconstruction of the winter NAO index since AD 1400, *J. Clim.*, *15*, 1754–1764.

Ding, Y., and T. Krishnamurti (1987), Heat budget of the Siberian High and the winter monsoon, *Mon. Weather Rev.*, *115*, 2428–2449.

Gong, D.-Y., and C.-H. Ho (2002), The Siberian High and climate change over middle to high latitude Asia, *Theor. Appl. Climatol.*, *72*, 1–9.

Hurrell, J. W. (1995), Decadal trends in the North Atlantic Oscillation and relationships to regional temperature and precipitation, *Science*, *269*, 676–679.

Jhun, J.-G., and E.-J. Lee (2004), A new East Asian winter monsoon index and associated characteristics of the winter monsoon, *J. Clim.*, *17*, 711–726.

Jones, P., and A. Moberg (2003), Hemispheric and large-scale surface air temperature variations: An extensive revision and an update to 2001, *J. Clim.*, *16*, 206–223.

Kripalani, R., and A. Kulkarni (1999), Climatology and variability of historical Soviet snow depth data: Some new perspectives in snow-Indian monsoon teleconnections, *Clim. Dyn.*, *15*, 475–489.

Kumar, K., B. Rajagopalan, and M. Cane (1999), On the weakening relationship between the Indian monsoon and ENSO, *Science*, *284*, 2156–2159.

Mann, M. E., and J. Lees (1996), Robust estimation of background noise and signal detection in climatic time series, *Clim. Change*, *33*, 409–445.

Meeker, L., and P. Mayewski (2002), A 1400-yr high-resolution record of atmospheric circulation over the North Atlantic and Asia, *Holocene*, *12*, 257–266.

Morinaga, Y., S. Tian, and M. Shinoda (2003), Winter snow anomaly and atmospheric circulation in Mongolia, *Int. J. Clim.*, *23*, 1627–1636.

Nakamura, H., T. Izumi, and T. Sampe (2002), Interannual and decadal modulations recently observed in the Pacific storm track activity and east Asian winter monsoon, *J. Clim.*, *15*, 1855–1874.

Panagiotopoulos, F., M. Shahgedanova, A. Hannachi, and D. Stephenson (2005), Observed trends and teleconnections of the Siberian High, *J. Clim.*, in press.

Sahsamanoglou, H., T. Makrogiannis, and P. Kallimopoulos (1991), Some aspects of the basic characteristics of the Siberian anticyclone, *Int. J. Clim.*, *11*, 827–839.

Trenberth, K. (1990), Recent observed interdecadal climate changes in the Northern Hemisphere, *Bull. Am. Meteorol. Soc.*, *71*, 988–993.

Trenberth, K., and D. Paolino (1980), Northern Hemisphere sea-level pressure data set: Trends, errors and discontinuities, *Mon. Weather Rev.*, *108*, 855–872.

Wu, B., and J. Wang (2002), Winter Arctic Oscillation, Siberian High and east Asian winter monsoon, *Geophys. Res. Lett.*, *29*(19), 1897, doi:10.1029/2002GL015373.

Yihui, D. (1990), Build up, airmass transformation and propagation of the Siberian High and its relation to cold surge in east Asia, *Meteorol. Atmos. Phys.*, *44*, 281–292.

Zhang, Y., K. Sperber, and J. Boyle (1997), Climatology and interannual variation of the east Asian winter monsoon: Results from 1979–95 NCEP/NCAR reanalysis, *Mon. Weather Rev.*, *125*, 2605–2619.

R. D'Arrigo and G. Jacoby, Lamont-Doherty Earth Observatory, P.O. Box 1000, Route 9W, Palisades, NY 10964, USA. (rdd@ldeo.columbia.edu)

F. Panagiotopoulos, Department of Geography, University of Reading, Reading, RG6 6AH, UK.

R. Wilson, School of Geosciences, Grant Institute, University of Edinburgh, West Mains Road, Edinburgh, EH9 3JW, UK.